PCCP

PAPER

View Article Online
View Journal | View Issue

Cite this: *Phys. Chem. Chem. Phys.*, 2015, **17**, 1290

Magnetic and geometric anisotropy in particle-crosslinked ferrohydrogels

Lisa Roeder,[a] Philipp Bender,[b] Matthias Kundt,[a] Andreas Tschöpe[b] and Annette M. Schmidt*[a]

Received 4th October 2014,
Accepted 12th November 2014

DOI: 10.1039/c4cp04493b

www.rsc.org/pccp

Particle-crosslinked polymer composites and gels have recently been shown to possess novel or improved properties due to a covalent particle–matrix interaction. We employ spindle-like hematite particles as exclusive crosslinkers in poly(acrylamide) gels, and exploit their extraordinary magnetic properties for the realization of ferrohydrogels with a perpendicular orientation of the preferred magnetic and geometric axes of the particles. The angle-dependent magnetic properties of uniaxially oriented gels are investigated and interpreted with respect to particle–matrix interactions. The impact of the particle orientation on the resulting angle-dependent magnetic performance reveals the presence of two different contributions to the magnetization: a hysteretic component ascribed to immobilized particles, and a pseudo-superparamagnetic, non-hysteretic component due to residual particle mobility. Furthermore, a plastic reorientation of magnetic particles in the matrix when subjected to a transversal field component is observed.

Introduction

For nanostructured hybrid materials, such as polymer composites, particle filled gels, and even biological systems, knowledge of the interaction mechanisms between solid filler particles and the polymer matrix is of great importance for understanding the structure and performance of the respective materials, and for allowing their optimization for distinct applications.[1–7] Magnetic nanoparticulate probes have recently been proven useful in supplying information on the specific particle environment using quasi-static[8–10] or dynamic[11–13] magnetic methods. Suitable for this purpose are particles with sufficient magnetic (or shape) anisotropy to allow their magneto-mechanical manipulation. They can be either spherical,[8,14] elongated[9] or platelet-shaped, and are usually based on iron oxides, ferrites, or metals.

Recently, the spindle-like hematite particles first described by Matijevic *et al.*[15] have been experiencing a growing popularity as components in hybrid materials. This is fostered by their easy synthesis in a variety of aspect ratios, their chemical and colloidal stability, and their valuable magnetic properties.[16–19]

The weak ferromagnetic behavior observed in natural and synthetic hematite originates from a canted antiferromagnetism. The antiferromagnetic coupling between alternating basal planes of the corundum crystal structure is slightly canted due to anisotropic exchange interaction (Dzyaloshinsky–Moriya interaction). This results in a residual magnetic moment perpendicular to the *c*-axis of the crystal. With respect to the deflection of this magnetic moment out of plane, hematite can be considered as a hard magnetic material, as has been demonstrated by many experimental studies and calculations.[16,20–23]

In spindle-like hematite particles prepared by thermolysis of aqueous $FeCl_3$ solution in the presence of NaH_2PO_4, the *c*-axis is oriented along the long geometric axis of the spindles. Thus they possess a magnetic moment perpendicular to their long axis. This behavior is extraordinary among nanomagnetic materials, as elongated nanoparticles are usually magnetized preferentially along their long axis due to the predominance of shape anisotropy. In the hematite spindles however, the crystal anisotropy or magnetoelasticity dominates the shape effect as a result of the low overall magnetization of the material.[10,18,19] A similar observation was also reported for Goethite-based nanomaterials.[24] The magnetic behavior of these particles, in particular their magnetic anisotropy within the basal planes, is not fully understood. The experimental evidence has been interpreted as pointing to either a triaxial or plane anisotropy as would be expected from the crystal structure, or to a uniaxial configuration possibly to be ascribed to magnetoelastic interactions.[18,23,25]

Nanoparticles covalently attached to polymeric matrices and gels and acting as particular crosslinkers have recently been shown to comprise improved mechanical properties and/or novel (magneto-)mechanical coupling effects as compared to their conventional analogs without covalent interphase links.[1,13,26–31] Building on our previous work on particle-crosslinked ferrohydrogels based on spherical $CoFe_2O_4$ particles in a poly(acrylamide)

[a] *Department Chemie, Institut für Physikalische Chemie, Universität zu Köln, Luxemburger Str. 116, D-50939 Köln, Germany. E-mail: annette.schmidt@uni-koeln.de*
[b] *Technische Physik, Universität des Saarlandes, Postfach 151150, D-66041 Saarbrücken, Germany*

(PAAm) matrix,[8,32] spindle-like hematite particles are used as exclusive crosslinkers in PAAm gels. As shown in a previous paper,[33] these gels can be synthesized in a wide range of compositions, and show an interesting viscoelastic behavior.[34]

The present study aims at the investigation of the angle-dependent magnetic properties of uniaxially oriented particle-crosslinked polymer hydrogels, and at interpreting the data with respect to the particle–matrix interaction. The particles are surface-functionalized and incorporated covalently into PAAm hydrogels as particulate crosslinkers. The particle orientation and its impact on the resulting magnetic performance in dependence on the angle between the gel axis and the field direction is examined in particle dispersion, and in soft and hard particle-crosslinked gels.

Experimental

Chemicals

Acrylamide (AAm) was purchased from Merck in p.a. quality. Sodium dihydrogenphosphate monohydrate ($NaH_2PO_4 \cdot H_2O$, p.a.) was obtained from AppliChem. 3-(Trimethoxysilyl)propyl methacrylate (MTS, $\geq$98%) and tetramethylammonium hydroxide (TMAOH, 25% in water) were obtained from Sigma-Aldrich. Ammonium peroxodisulfate (APDS) and *N*,*N*,*N*′,*N*′-tetramethylethylenediamine (TEMED) were purchased from Acros Organics in p.a. quality. Iron(III) chloride hexahydrate (98%, ABCR GmbH) and citric acid monohydrate (p.a. quality, Jungbunzlauer GmbH) were used without further purification. Ethanol was obtained from Hofmann Chemie AG in technical quality and distilled before use. The water used for sample preparation and analysis was obtained from Acros Organics in analytical quality.

Material constants from literature used in this study are the specific monomer density (ρ_{AAm} = 1.13 g cm^{-3}), the specific density of hematite ($\rho_{Fe_2O_3}$ = 5.256 g cm^{-3}),[16] and the literature value for the M_s of hematite is 2048 A m^{-1}.[35]

Instrumentation

Quasi-static magnetometry was performed on an ADE Magnetics Vibrating Sample Magnetometer (VSM) EV7. The magnetization curves were monitored at 298 K with a head drive frequency of 75 Hz on samples sealed in Teflon vessels and placed on a glass sample holder between two poles of an electromagnet. The field range of the instrument is −2.2 to 2.2 T. The angle-dependent magnetization curves were obtained by variation of the angle θ between the magnetic field vector applied during the measurement and the *z*-axis of the sample (direction of field employed during synthesis). Field vectors perpendicular to the *z*-axis of the sample are marked by θ_{xy} (*x* being the direction opposing gravity), whereas vectors within the *zy*-plane are marked by θ_{zy} (θ_{zy} = 0 being the *z*-axis) (Fig. 4a).

Scanning electron microscopy (SEM) images were taken on a Zeiss Neon 40 ESB CrossBeam FIB-SEM with a silicon wafer as sample holder.

Transmission electron microscopy (TEM) images were taken on a Zeiss LEO 912 Omega. The particle sample was prepared by drop-casting from diluted aqueous dispersion onto a copper grid with a carbon-hole film.

Orientation experiments were performed by drop-casting on a Si wafer placed between the pole shoes of a PHYWE electromagnet (06480.01) with pole pieces. The field strength was measured with a Magnet-Physik teslameter FH55 and regulated by a PHYWE power supply (13531.93). The dried samples were analyzed with SEM.

The Si content of functionalized particles was determined photometrically at Mikrolab Kolbe, Mülheim/Ruhr, Germany, on a Lambda 800 spectrometer (Perkin Elmer). Two individual high-pressure-digestions of carefully dried samples were quantified by a modified phosphor blue method.

Synthesis

The spindle-like hematite particles with surface-attached polymerizable groups were synthesized according to a three-step route described in detail in our previous paper.[33] The particle synthesis was based on the thermolysis of aqueous ferric chloride ($FeCl_3$, c = 0.02 mol L^{-1}) in the presence of NaH_2PO_4 ($c = 0.40 \times 10^{-3}$ mol L^{-1}) initially reported by Matijevic *et al.*[15] After thorough washing, the particles were electrostatically stabilized with citric acid and TMAOH in water (Fe_2O_3@CA).[36] In order to immobilize methacrylate groups on the particle surface, the particles were modified with MTS in ethanol at ambient temperature ($c_{Fe_2O_3}$ = 1.9 g L^{-1}, c_{MTS} = 0.036 mol L^{-1}),[32,37] washed with and redispersed in water (Fe_2O_3@MTS).

The synthesis of particle-linked gels was performed according to the method by free-radical polymerization of AAm in water in the presence of the functionalized particles.[8,32,33] A solution of a predetermined amount of monomer and particles in water (57 µl), initiator solution (APDS aq., 1.5 µL, c = 0.27 mol L^{-1}) and sensitizer (TEMED aq., 1.5 µL, c = 0.35 mol L^{-1}) were precooled to 4 °C, mixed in a precooled VSM container, and placed in a homogenous field of 468 kA m^{-1}. The polymerization was initiated by letting the mixture warm up to ambient temperature and was completed after 2 h. The particle volume fraction was $\nu_P = 1.6 \times 10^{-2}$ in all samples. The volume fraction of the monomer acrylamide in the polymerization mixture for the hard gel labelled as $FHG_{468}(22)$ is ν_M = 0.22. For the soft gel $FHG_{468}(11)$, the monomer fraction was decreased (ν_M = 0.11) at comparable particle fraction ($\nu_P = 1.6 \times 10^{-2}$). One isotropic hard gel $FHG_0(22)$ was prepared by polymerization in absence of an external field.

Results

Motivation and concept

The employment of spindle-like hematite nanoparticles as magnetic particulate crosslinkers in acrylamide-based hydrogels aims at the combination of conveniently available and manageable particles with an interesting geometry and the option of magnetic manipulation and read-out of the matrix. The synthetic procedures are readily available and allow a wide range of gel compositions.[33] However, while particles recently used for the

extraction of magnetomechanical characteristics in soft matrices are predominantly uniaxial and thus allow to model their properties on the base of an extended Stoner–Wohlfarth model,[9,38] the hematite spindles do not necessarily follow this behavior. While for perfectly uniaxial, non-interacting and statistically oriented Stoner–Wohlfarth particles a relative remanence M_r/M_s = 0.5 is expected, literature values for the hematite spindles vary between 0.50 and 0.78, pointing to a more or less triaxial anisotropy in the basal planes. In addition, the magnetically preferred axis or plane is not identical with the geometric main axis, as in the majority of other anisotropic magnetic particles. The resulting properties are thus complex with no suitable model available to date. In the present study, a comparison is made of the magnetic properties of the particles in three states: in aqueous dispersion (reference state with ν_M = 0), as covalent crosslinkers in a hard PAAm hydrogel, where the particles are strongly immobilized in the polymeric gels due to the high monomer fraction (ν_M = 0.22), and as crosslinkers in a soft PAAm gel (ν_M = 0.11) where the particles have the option to partly rotate under the influence of an external magnetic field. Polymerization of the two gels was performed in the presence of a homogenous magnetic field, resulting in a preferred uniaxial, magnetic orientation of the particles within the gel. For similar gels based on Ni rods, oriented in gelatin gels, it was shown that angle-dependent magnetization curves give insight into the local particle rotational deflection in the field.[38]

For the aqueous particle dispersion, it is possible to obtain information on the orientation degree as a function of the magnetic field strength by drop-casting experiments, and to show that the relation can be approximated by the magnetization curve of the fluid, in accordance with recent literature findings.[19,23,39]

The gels were prepared by the synthetic route displayed in Fig. 1. Spindle-like hematite particles were obtained by the Matijevic route[15] by aqueous thermolysis of ferric chloride in the presence of sodium dihydrogen phosphate, stabilized by subsequent addition of citric acid and TMAOH,[36] and functionalized with 3-(trimethoxysilyl)propyl methacrylate (MTS).[37] The latter step results in a thin shell of a crosslinked polysiloxane with pending methacrylate groups. In the following free-radical solution polymerization of AAm, the cores can thus act as particulate crosslinkers by a grafting-through process.[33] Variation of the monomer concentration allows the realization of gels with different mechanical properties, and a uniaxial magnetic orientation of the hematite spindles within the gels is possible by means of applying an external homogeneous magnetic field.

Particle characteristics. A TEM image of the α-Fe_2O_3 spindle-like particles is presented in Fig. 2a. The particles appear clearly contrasted with uniform shape. By measuring >100 particles

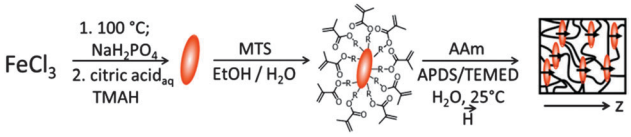

Fig. 1 Schematic illustration of the synthesis route; R = $(CH_2)_3SiO$, *Z*: direction of field *H* applied during synthesis.

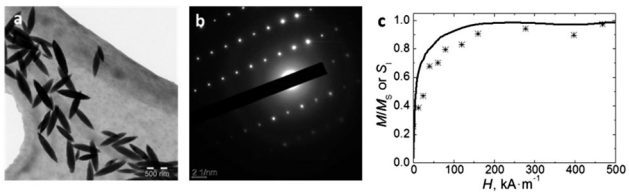

Fig. 2 (a) TEM-image and (b) electron diffraction pattern of Fe_2O_3@CA. (c) Orientation parameter S_I (points), and magnetization curve $M(H)/M_s$ obtained from quasi-static magnetometry in dispersion (solid line) as a function of the applied magnetic field *H*.

the determined average length *L* is 438 ± 88 nm and the average diameter 2*R* is 96 ± 18 nm. From these values a mean aspect ratio *n* = 4.6 ± 0.5 and a mean geometrical volume V_g of 2.1×10^{-21} m^3 with $V_g = 4/3 \cdot \pi \cdot (R)^2 \cdot (L/2)$ (ellipsoid) can be deduced. The electron diffraction pattern indicates that the particles are single crystals (Fig. 2b) and confirm the orientation of the crystal *c*-axis along the mean spindle axis.

After functionalization with MTS the amount of Si is determined by elemental analysis, indicating a functionalization degree *f* (given as the number of methacrylate groups per mass unit of particles) of 0.216 mmol g^{-1}. The theoretical number of methacrylate groups of a monolayer on the particle's surface is in the range of $\phi_{max} = 3 \times 10^5$ per particle, when a mean area per methacrylate group of 0.35 nm^{-2} is assumed.[37] Thus a thin shell of about five siloxane layers can be assumed, which is too thin to be detected by TEM.[40] As each methacrylate group, if polymerized, links two network segments to the particle, the maximum crosslinker functionality of the average particle is high with at least 6×10^5.

ν_M = 0: field-dependent particle orientation in aqueous dispersion. While a principal magnetic order parameter of the magnetic moments in dispersion can be obtained from the magnetization curve of the dispersion, the direction and extent of particle orientation and their spatial distribution under the influence of an external magnetic field between 0 and 468 kA m^{-1} is visualized from drop-casting under field influence with SEM. Exemplary images of the two-dimensional projection are displayed in Fig. 3a–c. They clearly indicate that the particles are mostly isolated from each other, and that bigger aggregates are absent. As expected, increasing field-strength leads to the particles orienting their long axis perpendicularly to the field direction.[18,19,23]

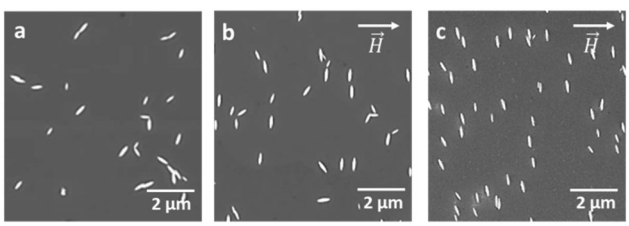

Fig. 3 SEM-images of spindle-like particles Fe_2O_3@MTS, samples prepared at different magnetic field strength (a) *H* = 0 kA m^{-1}, (b) *H* = 79 kA m^{-1} and (c) *H* = 468 kA m^{-1}.

For a semi-quantitative analysis, an orientational order parameter S_l is defined in accordance to the definition used in nematic phases[41–44]

$$S_l = \left\langle \frac{3\sin^2\beta - 1}{2} \right\rangle \quad (1)$$

with β: angle between the main geometrical axis $\vec{l}$ and the director given by the external field vector $\vec{H}$. As in an ideally ordered sample the axis is perpendicular to the director, S is expressed on the basis of $\sin\beta$ instead of the commonly employed cos function, when (molecular) axes and the director are expected to be parallel for a fully ordered case.

S_l is determined for each of the samples prepared at different field strengths H by taking into account at least 100 particles. As seen in Fig. 2c, S_l steadily increases with H, and for moderate fields higher than 278 kA m^{-1}, a maximum ordering of the particles is achieved. The results of S_l are only an approximation due to the indirect imaging method, but give a more precise estimation of the qualitative course of the geometrical particle orientation with applied magnetic field strength.

To further underline afore mentioned results, the relation can be compared to the normalized magnetization curve $M(H)/M_s$ of the particle dispersion obtained from VSM. It is taken into account that the field-dependent relative sample magnetization $M(H)/M_s$ is a measure of the magnetic degree of order in non-hysteretic magnetic materials.

According to the VSM results, the particle dispersions show a pseudo-superparamagnetic behavior, indicated by the absence of hysteresis. This is readily explained by the rotational freedom of the particles on the time scale of the experiment, allowing a fast and unhindered magnetic orientation in the field by Brownian rotation. The orientation is counteracted by thermal motion in terms of k_BT and is thus fully reversible as long as the particles are well-dispersed. The saturation magnetization of the fluid is in accordance with the particle concentration. From the initial susceptibility based on the Langevin function, an average magnetic particle moment μ_P of 1.1×10^{-18} A m^2 can be calculated. It is in reasonable agreement with the expectation from the mean geometrical particle volume V_g 2.1×10^{-21} m^3 and the measured saturation magnetization of hematite, M_0 = 1.2 kA m^{-1}, resulting in $\mu_P = M_0 \cdot V_g = 2.6 \times 10^{-18}$ A m^2.[16]

Accordingly, the normalized experimental magnetization curve represents the magnetic order parameter $S_m = M(H)/M_s$ by means of exemplifying the projection of the first magnetic moment of the orientation distribution to the field axis. Thus, it can be compared to the geometric order parameter S_l. Between the geometric order parameter S_l and the magnetic analogue S_m, a qualitative compliance is observed in their field strength dependence. The geometric order parameter increases more slowly with the magnetic field strength than the magnetic parameter S_m. Though the ratio S_l/S_m is field-dependent, and increases from 0.5 for small fields to nearly 1 at fields >278 kA m^{-1}. Part of the difference may be ascribed to methodical differences and to the fact that for the geometrical analysis a 2D projection of a drop-casted sample is used. To a certain extent it is also expected from theoretical considerations, as a magnetic orientation of the particles along the field axis (z-axis) is for the present particle geometries accompanied by a preferred geometrical orientation with the long spindle axis perpendicular to the field (see Fig. 4a). However the orientation within the xy-plane remains undetermined, if the particle fraction is low enough to exclude magnetic or hydrodynamic particle interactions.

In either case, the simple orientation experiment principally confirms the degree of particle orientation in fields with varying strength, and is in agreement with the relative configuration of magnetic moment with respect to the geometric shape.

Angle-dependent magnetization curves of particle-crosslinked ferrohydrogels. While the spindle-like particles display free rotation and statistic orientation in aqueous dispersion, their incorporation into particle-crosslinked gels is expected to result in a more or less complete immobilization. In order to obtain more detailed information on the particle mobility in such gels, the angle-dependent magnetic properties of three gels with varying monomer fraction ν_M are compared: one hard, isotropic gel [ν_M = 0.22; labeled as FHG$_0$(22)], and two uniaxially magnetized gels of soft and hard nature synthesized in the presence of an applied magnetic field of 468 kA m^{-1}. The gels are labelled as FHG$_{468}$(11) for the soft and FHG$_{468}$(22) for the hard sample. The description of ''soft'' and ''hard'' results from the expected degree of particle–matrix interaction or particle immobilization.

For each of the gels, magnetization curves are collected and analyzed with varying angles θ, with respect to the initial/magnetic field vector H during synthesis. The results support the expected magnetic axis of the gels. In the applied coordinate system this axis is the z-axis (Fig. 4a). The yz-plane as well as the xy-plane, the latter being perpendicular to the magnetic axis, are investigated this way.

ν_M = 0.22: the isotropic, hard gel FHG$_0$(22). The angle-dependent magnetization curves of an isotropic, particle-crosslinked ferrohydrogel prepared with a high monomer volume fraction of ν_M = 0.22 at different angles θ between 0 and 90° in the xy as well as in the zy-plane are shown in Fig. 4b. The curves are almost identical, and confirm the isotropic particle distribution within the sample with respect to particle concentration and orientation. All curves show a distinct hysteresis with a coercive field strength of H_C = 40 kA m^{-1} and a remanence M_r/M_s = 0.6, in agreement with recent results of immobilized hematite nanoparticles.[19,25]

With respect to theoretical considerations, the corundum structure of the particles and the canted antiferromagnetic coupling pattern give rise to a magnetic structure with a preferred magnetic orientation within the basal plane. As this plane itself is of triaxial symmetry, three configurations of easy magnetization cases can be considered:

(a) three equivalent magnetic axes within the basal plane with an angle of 60° (triaxial anisotropy),

(b) no preferred axis within the plane due to low crystal anisotropy constant (plane anisotropy),

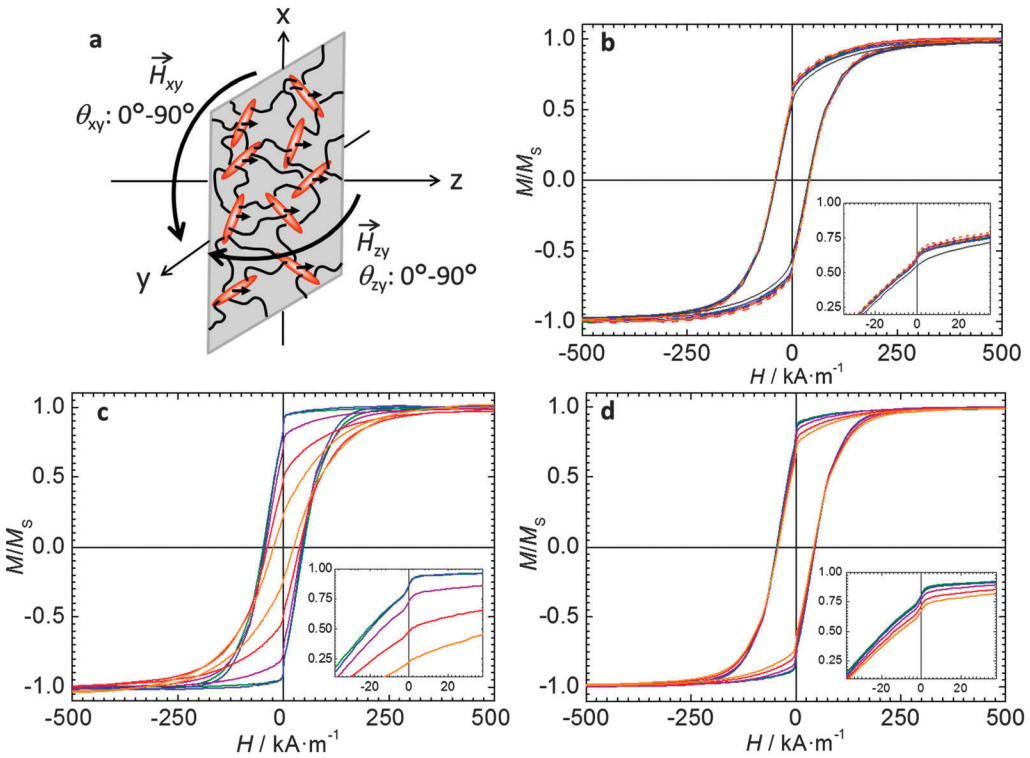

Fig. 4 (a) Schematic illustration of the setup geometry and axes annotations. Magnetization curves of (b) the isotropic hard gel $FHG_0(22)$ in comparison with the particles measured as powder (grey); (c) the anisotropic hard gel $FHG_{468}(22)$; (d) the anisotropic soft gel $FHG_{468}(11)$; solid line: *zy*-plane, dashed line: *xy*-plane; θ_{xy} or θ_{zy}: 0° (green), 22.5° (blue), 45° (purple), 67.5° (red), 90° (orange).

(c) one of the crystal axes within the basal plane dominates, resulting in uniaxial, magnetic anisotropy.

While in the latter case (c) the magnetic behavior could be principally described by a Stoner–Wohlfarth model and we would expect a remanence of 0.5,[9,45] in the case (a) the triaxial anisotropy within the basal plane results in a theoretical remanence M_r/M_s of 0.75.[18,25,46] In case (b), the existence of an easy plane would allow an easy adjustment of the particle magnetic moment within all field directions in an isotropic sample, and is thus not in accordance with a strong hysteresis.

The experimental value for M_r/M_s in the hard isotropic sample is thus between the theoretical expectations for the uniaxial, and the triaxial, magnetic anisotropy.

The reproducibility and the reversibility of the magnetic behavior with respect to consecutive hysteretic cycles has readily been confirmed. By further analysis in terms of a ΔM plot ($\Delta M(H) = M(H)_{virgin} - 0.5[M(H)_{upfield} + M(H)_{downfield}]$; Fig. 5a), it can additionally be shown that the initial magnetization during the first branch does not lead to particle interactions or irreversible collective changes in the relative particle configuration.[47]

One peculiarity is observed in all magnetization graphs of $FHG_0(22)$ at low field strength. A deviation from usual hysteretic behavior at small fields is observed, which can be explained by an underlying, non-hysteretic (pseudo-superparamagnetic) magnetization curve with low intensity. Such a non-hysteretic portion of magnetization M_{sp} in the particle-crosslinked gel,

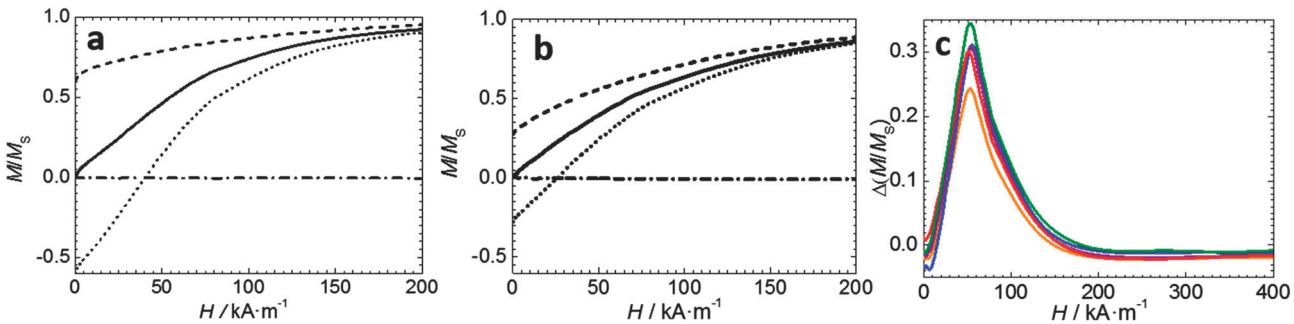

Fig. 5 Magnetization curves and ΔM plots of (a) $FHG_0(22)$ at θ_{zy} = 0° and (b) $FHG_{468}(22)$ θ_{xy} = 0°; (c) angle-dependent ΔM plots of $FHG_{468}(11)$ with θ_{zy}: 0° (green), 22.5° (blue), 45° (purple), 67.5° (red), 90° orange).

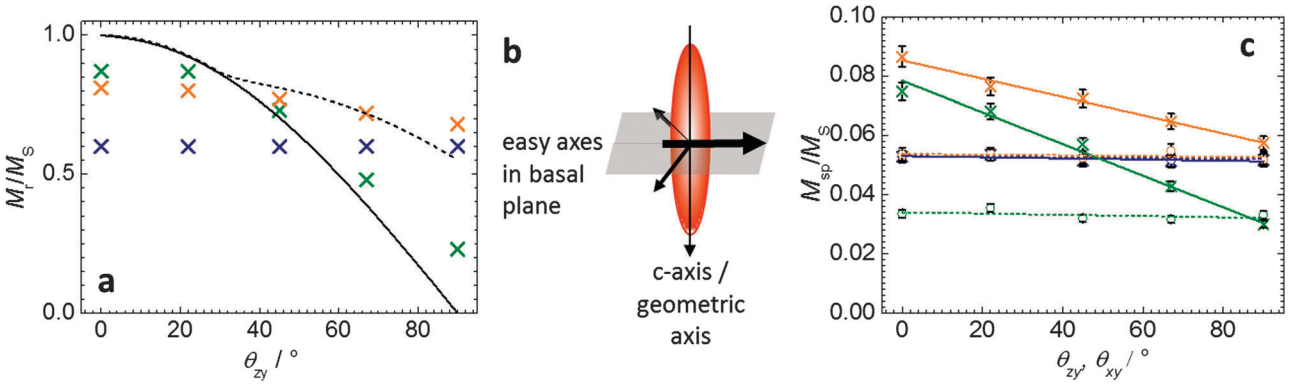

Fig. 6 (a) Angle-dependent normalized remanence M_r/M_s of the gels in the *zy*-plane in comparison with theoretical calculations (line: theoretical uniaxial anisotropy, dashed line: theoretical triaxial anisotropy; (b) crystal and shape anisotropy axes in a spindle-like particle; (c) angle-dependent non-hysteretic portion of the magnetization M_{sp}/M_s in the *zy*-plane (crosses, solid lines) and the *xy*-plane (circles, dashed lines); $FHG_{468}(22)$ (green), $FHG_{468}(11)$ (orange), $FHG_0(22)$ (blue).

that is not observed if the particles are analyzed as a powder, can be ascribed to a quasi-superparamagnetic contribution due to residual particle mobility within the gels. In the present case, this portion M_{sp} of the overall magnetization M_s amounts to 5.3%, independent of the measuring angle (Fig. 6c). Thus, in the gel, the immobilization of the particles cannot be fully achieved.

ν_M = 0.22: the uniaxial, hard gel $FHG_{468}(22)$. A gel with the aforementioned composition, but prepared under the influence of a homogeneous external magnetic field of 468 kA m^{-1} is subjected to the same angle-dependent magnetization experiment. All axes are named within the gel-centered coordination system, with the *z*-axis pointing in the direction of the field applied during synthesis, and a vertical *x*-axis (Fig. 4a). The angle θ_{zy} is defined relative to the *z*-axis of the gel in the *zy*-plane, and θ_{xy} indicates the angle perpendicular to this axis. As can be observed in Fig. 4c, the normalized magnetization curves in the *zy*-plane are angle-dependent, and their coercive field strength and remanence decrease with the measurement angle deviating from the field direction during the synthesis (*z*-axis of the gel). In contrast, all magnetization graphs in the *xy*-plane (not shown) are consistent, and as expected from symmetry considerations, they are also consistent with the curve at $\theta_{zy} = 90°$.

All measurements are reproducible as well on this specific sample as on newly synthesized material. The ΔM plot of the gel performed for two angles perpendicular to the *z*-axis for each gel ($\theta_{zy} = 90°$, $\theta_{xy} = 0°$, Fig. 5b) also confirms the absence of irreversible changes to the sample during the first magnetization cycle.

The angle-dependence of M_r/M_s can be compared to the theoretical expectation for a triaxial and a uniaxial, magnetic anisotropy of the particles (cases (a) and (c), see above) under the assumption that they are predominantly immobilized in the gel matrix. For both cases, one would ideally expect a maximum $M_r/M_s = 1$ for fully oriented and immobilized particles at $\theta_{zy} = 0°$. For the uniaxial case, the remanence follows $\cos\theta_{zy}$,[38,45] and decreases to 0 for $\theta_{zy} = 90°$. The expected angle-dependent remanence for a triaxial anisotropy is calculated by assuming that within the ensemble of immobilized particles, the orientation of the main particle axis is preferably in the *xy*-plane of the gel. Thus the basal plane orientation is statistically distributed with respect to *z*. Further, we assume that $k_BT \ll E_{m,basal} \ll E_{m,c}$, and that the magnetic moments flip or return to the closest anisotropy axis at $H = 0$ kA m^{-1} (see Appendix). The decrease of M_r/M_s with θ_{zy} is less steep in the triaxial case, with a value of 0.55 reached at $\theta_{zy} = 90°$ (Fig. 6a). The experimental results for M_r/M_s in the *zy*-plane decrease continuously from 0.87 to 0.23. Thus these are not sufficiently explainable with neither model, in accordance with the observations on the isotropic sample.

For small field strengths, the curves indicate the presence of a non-hysteretic component, similar to the observations in the isotropic sample. Within the *xy*-plane, thus perpendicular to the gel magnetization during synthesis, this component of the magnetization M_{sp}/M_s is about 3.2% irrespective of the measuring angle. Thus the values are lower than observed for the isotropic sample. However, in the *zy*-plane, an interesting course with the angle is observed, a linear decrease of the non-hysteretic fraction from 7.5% to 3.2% with increasing θ_{zy} (Fig. 6c). This non-hysteretic magnetic component reflects the residual mobility of the particles within their specific environment with respect to orientation under an applied field. Compared to the isotropic sample, the residual particle mobility is increased parallel to the initial field (*z*-axis) while it is reduced perpendicular to it. While this finding is counter-intuitive, it reflects the particles' preferred geometrical orientation in the gel: the long axis of the particles is pointed normal to the axis in the preferential orientation, allowing a partial remagnetization by rotation along the long axis (small mechanical moment) when the magnetization is reversed, while in the *xy*-plane a rotation along the short axis (high mechanical moment) is necessary to allow a magnetization reversal.

ν_M = 0.11: the uniaxial, soft gel $FHG_{468}(11)$. When the gel is prepared with a lower monomer concentration, the immobilization of the particles within the gels is expected to be less effective with respect to remagnetization. To investigate the impact on the magnetic performance, the angle-dependent magnetization curves were recorded on a gel with a polymer fraction cut by half (ν_M = 0.11), but comparable particle content (ν_P = 0.0159).

The resulting magnetization curves are shown in Fig. 4d. While the curves within the *xy*-plane are again similar with a remanence of 0.67 (not shown), the differences between the curves in the *zy*-plane are less pronounced than for the harder uniaxial gel.

The angle-dependent remanence of the gel is shown in Fig. 6a. In comparison to the expectations for fully immobilized particles with uniaxial and triaxial geometry, the angle dependence is lower than expected. While for small angles, the remanence is similar to the values for the hard anisotropic gel $FHG_{468}(22)$, the remanence hardly decreases with θ_{zy}, remaining at high level also for a field orientation perpendicular to the initial axis. The coercive field is similar for all angles at 40 kA m^{-1}.

As already observed for the hard gels, the curves indicate the presence of a non-hysteretic component as observed by the step at zero field. The portion of non-hysteretic magnetization M_{sp}/M_s is nearly constant for all angles θ_{xy} in the *xy*-plane at about 5.5%. In the *zy*-plane, M_{sp}/M_s increases significantly from 5.5% to 8.7% with decreasing angle to the *z*-axis. The findings thus confirm the results for the hard isotropic gel, indicating a comparably higher residual particle mobility.

A ΔM analysis is provided for different angles θ_{zy} within the *zy*-plane (Fig. 5c). In contrast to both the isotropic and the uniaxial, hard gel, all curves obtained for the soft gel comprise a non-vanishing, positive residue when comparing the sum of the upfield and downfield branch of the curves to the virgin curve after demagnetization. The positive residue indicates that the sample is easier magnetized in the first cycle (virgin curve) than in the following cycles, irrespective of the measuring angle, indicating the presence of irreversible changes within the material configuration during the first cycle. The maximum of the residue is located at $H \sim 50$ kA m^{-1}, close to the coercivity field.

Discussion

The detailed analysis of the angle-dependent properties of soft and hard, isotropic and uniaxial ferrohydrogels gives rise to the differentiation of at least two different magnetic components. First, in all the samples except the aqueous particle dispersion, a dominant hysteretic component is observed that is characterized by an angle-dependent remanence. This portion is ascribed to the internal remagnetization of predominantly immobilized, magnetically blocked particles that are remagnetized by internal reorientation against the crystal anisotropy. It is shown that the behavior cannot exactly be described neither by a uniaxial nor triaxial configuration of the magnetocrystalline anisotropy within the basal plane. According to the results for the gels with high monomer concentration (hard gels), however, the relation resembles a better correspondence with an uniaxial geometry of the magnetic anisotropy of the particles.

Further, we observe a portion of the magnetization that can be ascribed to residual particle mobility. This portion M_{sp}/M_s is higher in the soft than in the hard gels, and shows an angle-dependence for the uniaxial gels. It is higher for small angles close to the gel (*z*) axis – this may be ascribed to a preferential ordering of the particles with their long axis perpendicular to the magnetic axis. As a consequence, a remagnetization is possible by rotation along the long axis (small moment), while in experiments concerning angles perpendicular to the initial magnetization, a remagnetization would refer to a rotation along the short axis (large moment). The results are thus in accordance with the underlying network architecture.

The presence of a positive residue in the angle-dependent ΔM plots of the soft gels indicates a non-reversible (plastic) effect in the magnetization of this material. A plausible explanation is a plastic deformation of the particle orientation within the gel as a consequence of the first magnetization cycle after the demagnetization procedure. The reduced remanence of the soft gel is higher than for the isotropic gel at all angles, resulting in a weaker angle-dependence. The incorporation of the magnetically blocked particles into a soft matrix thus results in a material that shows a programmable, magnetic easy axis with a considerable switching field of $\sim$40 kA m^{-1} – the magnetic performance and anisotropy can be adjusted by the monomer concentration and swelling degree as well as the presence and strength of an external field during synthesis.

Conclusion

By angle-dependent magnetic experiments, a novel class of geometrically and magnetically anisotropic, particle-crosslinked ferrohydrogels is investigated. The particles employed are of spindle-like geometry with hematite as the core material, and possess a length of about 440 nm and an aspect ratio of 4.6 with a narrow size distribution. The canted antiferromagnetism of hematite with the corundum c axis oriented along the spindle axis results in a weak ferromagnetic behavior of the particles with a preferred direction of the magnetic moment perpendicular to the long particle axis. The particles can be oriented in magnetic fields of a few hundred kA m^{-1}, and are surface-functionalized with MTS to allow a grafting-through copolymerization.

Isotropic and anisotropic ferrohydrogels were prepared from surface-functionalized hematite spindles and acrymaide by the free-radical polymerization, resulting in magnetic particle-crosslinked ferrohydrogels.[33] By the application of an external magnetic field during the synthesis, anisotropic gels are obtained with different degrees of internal magnetic and geometric order. We identify two magnetic components that contribute to the angle-dependent behavior: one is of hysteretic nature and displays a behavior that is best (but not fully) described by an ensemble of particles with uniaxial crystal anisotropy immobilized in a matrix, displaying a preferred direction of magnetization.

A second component refers to the residual particle mobility within the gels, and is manifested in the non-hysteretic contribution to the magnetization curve. This component clearly depends on the monomer concentration. It shows a reasonable angle-dependence for the anisotropic gels that is in accordance with the orientation of the magnetic moment perpendicular to the geometric axis of the particles as well as the corresponding

orientation of the particles in the gel. Finally, a plastic orientation effect is identified within the soft anisotropic gel, indicating a soft material with hard (hysteretic) magnetic properties and an adaptive preferred magnetization axis.

Appendix

The calculation of the angle-dependent normalized remanence of uniaxially immobilized particles with a triaxial anisotropy within the basal plane is as follows. After magnetic orientation of the particles in the field direction θ_{zy}, and subsequent switch-off of the field, the magnetic moment flips back to the closest minimum energy state (or easy axis). In the proposed geometry, the easy axes are found at a distance of 60° within the basal plane. For symmetry reasons, two axes need to be taken into account ($\hat{e}_0$ or $\hat{e}_1$ in Fig. 7, with $\hat{e}_0$ being oriented in z direction). Up to θ_{zy} = 30°, $\hat{e}_0$ is always the closest energy minimum independent from the angle ϕ (orientation of the particle with respect to the x-axis). For $\theta_{zy} > 30°$ there is a critical angle ϕ^* above which $\hat{e}_1$ is the closest easy axis. The critical angle ϕ^* is calculated by

$$\phi^* = \arcsin\left(\frac{1}{\sqrt{3}\tan\theta_{zy}}\right) \quad \text{for } \theta_{zy} > 30° \qquad \text{(A1)}$$

and

$$\phi^* = 90° \quad \text{for } \theta_{zy} \leq 30°. \qquad \text{(A2)}$$

To obtain the resulting remanence for the particle ensemble, we integrate the projections of $\hat{e}_0$ (to ϕ^*) and $\hat{e}_1$ (above ϕ^*) for all possible particle orientations:

$$\frac{M_r}{M_S} = \frac{2}{\pi}\left(\int_0^{\phi^*} \hat{e}_H \cdot \hat{e}_0 \mathrm{d}\phi + \int_{\phi^*}^{\pi/2} \hat{e}_H \cdot \hat{e}_1 \mathrm{d}\phi\right). \qquad \text{(A3)}$$

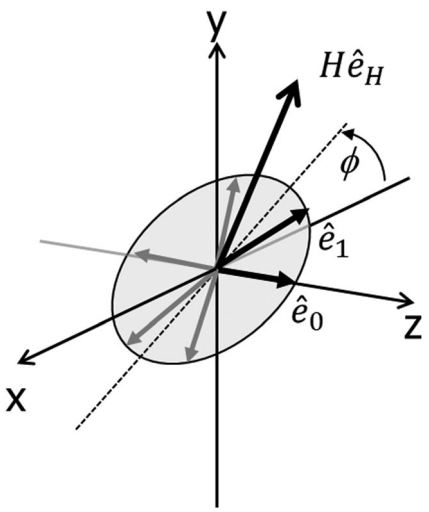

Fig. 7 Calculation of the angle-dependent normalized remanence with triaxial anisotropy. H is in the zy-plane with the angle θ_{zy} to the z-axis (not shown).

Acknowledgements

We would like to thank Ruth Bruker (Universität zu Köln) for SEM images and Lhoussaine Belkoura (Universität zu Köln) for TEM images. Furthermore we gratefully acknowledge the DFG (SPP 1259/1681) for financial support.

References

1 R. Messing and A. M. Schmidt, *Polym. Chem.*, 2011, **2**, 18.
2 P. Schexnailder and G. Schmidt, *Colloid Polym. Sci.*, 2009, **287**, 1–11.
3 S. Behrens, *Nanoscale*, 2011, **3**, 877–892.
4 A. Fernández-Barbero, I. J. Suárez, B. Sierra-Martín, A. Fernández-Nieves, F. J. de Las Nieves, M. Marquez, J. Rubio-Retama and E. López-Cabarcos, *Adv. Colloid Interface Sci.*, 2009, **147–148**, 88–108.
5 V. Thomas, M. Namdeo, Y. M. Mohan, S. K. Bajpai and M. Bajpai, *J. Macromol. Sci., Part A: Pure Appl.Chem.*, 2008, **45**, 107–119.
6 Y. Li, G. Huang, X. Zhang, B. Li, Y. Chen, T. Lu, T. J. Lu and F. Xu, *Adv. Funct. Mater.*, 2013, **23**, 660–672.
7 A. M. Schmidt, *Colloid Polym. Sci.*, 2007, **285**, 953–966.
8 N. Frickel, R. Messing and A. M. Schmidt, *J. Mater. Chem.*, 2011, **21**, 8466.
9 P. Bender, A. Tschöpe and R. Birringer, *J. Magn. Magn. Mater.*, 2013, **346**, 152–160.
10 L. Roeder, P. Bender, A. Tschöpe, R. Birringer and A. M. Schmidt, *J. Polym. Sci., Part B: Polym. Phys.*, 2012, **50**, 1772–1781.
11 V. L. Calero-DdelC, D. I. Santiago-Quiñonez and C. Rinaldi, *Soft Matter*, 2011, **7**, 4497.
12 C. Barrera, V. Florián-Algarin, A. Acevedo and C. Rinaldi, *Soft Matter*, 2010, **6**, 3662–3668.
13 E. Roeben, L. Roeder, S. Teusch, M. Effertz, U. K. Deiters and A. M. Schmidt, *Colloid Polym. Sci.*, 2014, **292**, 2013–2023.
14 J. a. Galicia, F. Cousin, E. Dubois, O. Sandre, V. Cabuil and R. Perzynski, *Soft Matter*, 2009, 2614–2624.
15 M. Ozaki, S. Krathovil and E. Matijevic, *J. Colloid Interface Sci.*, 1984, **102**, 146–151.
16 F. Bødker, M. F. Hansen, C. B. Koch, K. Lefmann and S. Mørup, *Phys. Rev. B: Condens. Matter Mater. Phys.*, 2000, **61**, 6826–6838.
17 R. D. Zysler, D. Fiorani, A. M. Testa, L. Suber, E. Agostinelli and H. Godinho, *Phys. Rev. B: Condens. Matter Mater. Phys.*, 2003, **68**, 212408.
18 Y. Zhao, C. W. Dunnill, Y. Zhu, D. H. Gregory, W. Kockenberger, Y. Li, W. Hu, I. Ahmad and D. G. McCartney, *Chem. Mater.*, 2007, **19**, 916–921.
19 M. Reufer, H. Dietsch, U. Gasser, B. Grobety, A. M. Hirt, V. K. Malik and P. Schurtenberger, *J. Phys.: Condens. Matter*, 2011, **23**, 065102.
20 A. H. Morrish, *Canted Antiferromagnetism: Hematite*, World Scientific Publishing Co. Pte. Ltd, Singapore, 1994.
21 I. Dzyaloshinsky, *J. Phys. Chem. Solids*, 1958, **4**, 241–255.
22 D. J. Dunlop, *Rep. Prob. Phys.*, 1990, **53**, 707–792.

23 M. Reufer, V. A. Martinez, P. Schurtenberger and W. C. K. Poon, *Langmuir*, 2012, **28**, 4618–4624.
24 B. J. Lemaire, P. Davidson, J. Ferré, J. P. Jamet, P. Panine, I. Dozov and J. P. Jolivet, *Phys. Rev. Lett.*, 2002, **88**, 125507.
25 Ö. Özdemir and D. J. Dunlop, *J. Geophys. Res.*, 2006, **111**, B12S03.
26 K. Haraguchi and T. Takehisa, *Adv. Mater.*, 2002, **14**, 1120–1124.
27 P. Ilg, *Soft Matter*, 2013, **9**, 3465–3468.
28 M. Feyen, E. Heim, F. Ludwig, A. M. Schmidt and D. Du, *Chem. Mater.*, 2008, 2942–2948.
29 T. Gelbrich, G. U. Marten and A. M. Schmidt, *Polymer*, 2010, **51**, 2818–2824.
30 F. Ludwig, A. Guillaume, M. Schilling, N. Frickel and A. M. Schmidt, *J. Appl. Phys.*, 2010, **108**, 033918.
31 M. Hod, C. Dobbrow, M. Vaidyanathan, D. Guin, L. Belkoura, R. Strey, M. Gottlieb and A. M. Schmidt, *J. Colloid Interface Sci.*, 2014, **436C**, 83–89.
32 R. Messing, N. Frickel, L. Belkoura, R. Strey, H. Rahn, S. Odenbach and A. M. Schmidt, *Macromolecules*, 2011, **44**, 2990–2999.
33 L. Roeder, M. Reckenthäler, L. Belkoura, S. Roitsch, R. Strey and A. M. Schmidt, *Macromolecules*, 2014, **47**, 7200–7207.
34 C. Gürler, M. Feyen, S. Behrens, N. Matoussevitch and A. M. Schmidt, *Polymer*, 2008, **49**, 2211–2216.
35 *The Landolt-Börnstein Database - Group III Condensed Matter, Numerical Data and Functional Relationships in Science and Technology*, Springer-Materials, 12b edn, http://www.springermaterials.com.
36 J. Wagner, T. Autenrieth and R. Hempelmann, *J. Magn. Magn. Mater.*, 2002, **252**, 4–6.
37 N. Frickel, R. Messing, T. Gelbrich and A. M. Schmidt, *Langmuir*, 2010, **26**, 2839–2846.
38 P. Bender, A. Günther, A. Tschöpe and R. Birringer, *J. Magn. Magn. Mater.*, 2011, **323**, 2055–2063.
39 M. Reufer, H. Dietsch, U. Gasser, A. Hirt, A. Menzel and P. Schurtenberger, *J. Phys. Chem. B*, 2010, **114**, 4763–4769.
40 G. Liu, L. Li and X. Yang, *Polymer*, 2008, **49**, 4776–4783.
41 W. Maier and A. Saupe, *Z. Naturforsch.*, 1959, **15A**, 882–889.
42 W. Maier and A. Saupe, *Z. Naturforsch.*, 1960, **14A**, 287–292.
43 S. K. Ghosh, *Nuovo Cimento*, 1984, **4D**, 229–244.
44 W. L. McMillan, *Phys. Rev. A: At., Mol., Opt. Phys.*, 1971, **4**, 1238–1246.
45 E. C. Stoner and E. P. Wohlfarth, *IEEE Trans. Magn.*, 1991, **27**, 3475–3518.
46 P. J. Flanders and W. J. Schuele, *Philos. Mag.*, 1964, **9**, 485–490.
47 S. Thamm and J. Hesse, *J. Magn. Magn. Mater.*, 1996, **154**, 254–262.

